Microneedle Array Integrated With CNT Nanofilters for Controlled and Selective Drug Delivery

Hao Wang, Zhuolin Xiang, Chih-Fan Hu, Giorgia Pastorin, Weileun Fang, *Senior Member, IEEE*, and Chengkuo Lee, *Member, IEEE*

***Abstract*— An innovative process of integrating microneedle array with carbon nanotube (CNT) nanofilters is developed for a novel transdermal drug delivery device with nanometer-scale selectivity and control mechanism. The SU-8 microneedle array is fabricated by the double drawing lithography process. This microneedle array is capable of penetrating stratum corneum (SC) layer. Then, drug molecules can selectively pass through CNT nanofilters with the aid of pressure, or an electric field, and are effectively delivered into the tissues under the SC layer. The CNT bundles integrated within the microneedle array act as nanofilters to block particles and molecules larger than the inner diameter of the CNTs. Moreover, the CNT nanofilters can selectively control the delivered drugs when they are under various electric fields. Three kinds of biomolecules, e.g., glucose, insulin, and hemagglutininare are investigated. The results demonstrate that the proposed novel transdermal drug delivery device can effectively deliver drug molecules in a selectively control mechanism. [2013-0366]**

***Index Terms*— Microneedle array, double drawing lithography, carbon nanotube (CNT) nanofilters, controlled and selective drug delivery.**

I. Introduction

MICRONEEDLES for transdermal drug delivery are promising devices to replace traditional hypodermic needles due to their minimally invasive procedure. There is a promising possibility for self-administration with a low risk of injuries [1]. It is more effective for pharmaceutical and therapeutic agents to be transported into the body via skin. Previously, various microneedles devices for transdermal drug delivery applications have been reported. They have been successfully fabricated by different materials and methods [2]–[24]. But none of them have integrated functions for controlled drug release with mechanical valves such as CNT nanofilters. Such a drug control releasing function is desirable for long term drug delivery and could expand the applications of microneedles. In this study, an innovative process to make SU-8 microneedles integrated with SU-8 sharp tips and vertical grown Carbon nanotubes (CNTs) bundles is developed. The CNT bundles are embedded within the SU-8 microneedles as the function of nanofilters. Nowadays the tubular structure of CNTs is a hot topic for mass transport. Gas, liquid and bimolecular have been proven to be capable of passing through the inner channel of CNTs [25]–[46]. Moreover, by using the unique property of nano-scale inner channels and the out surface which is easy to be modified, selective transport has been realized by surface modification [45], size exclusion [26] and DEP force alignment [46], showing the feasibility of using vertical aligned CNT forest as nanofilters for selective transport of drug molecules. Such nanofilters could realize the function of controlled selective drug release. The delivery of drugs of different molecular dimensions could be controlled by pressure and an electric field. In this study, a mixture of glucose and Hemagglutinin is used to demonstrate the function of selective drug delivery. Glucose and insulin of low molecular weight could pass through CNTs just by applying pressure. And due to the insulin molecules in solution are positively charged, the transport rate through CNT nanofilters could be tuned by electric field. Hemagglutinin, a kind of cylindrical molecule close to the inner diameter of the CNT inner channel, could pass through CNTs by applying electric field and pressure simultaneously [46], while glucose could be delivered when only pressure is applied. In the case that both pressure and electric field are given, both glucose and Hemagglutinin could be delivered.

The design of the microneedle array integrated with CNT nanofilters is shown in Fig. 1. An array of SU-8 microneedles was patterned above a SU-8 membrane(Fig. 1(a)). Every SU-8 microneedle has two parts: four-beam sidewalls at the bottom and a sharp tip at top as shown in Fig. 1(c). The four-beam sidewalls (brown parts in Fig. 1(a)) are patterned by photo lithography. The gaps along the sidewalls are the outlets of the microneedles. The sharp tips above the four-beam structure (green parts in Fig. 1(a)) are assembled and patterned by double drawing lithography. Above them, a layer of gold surface electrode was deposited onto the whole surface. This surface electrode allows us to apply an electric field in the test. Inside the four-beam structures, vertical grown CNT bundles (black parts in Fig. 1(a)) were embedded in the SU-8 membrane to form the CNT nanofilters. Fig. 1(d) shows the SEM image of one CNT bundle. Underneath the SU-8 membrane, there a SU-8 chamber layer to support the SU-8

Manuscript received November 28, 2013; revised April 17, 2014; accepted June 16, 2014. Date of publication August 14, 2014; date of current version September 29, 2014. This work was supported by the Ministry of Education, Academic Research Fund-Tier 2, through the Nanoneedle Devices for Transdermal Vaccine Delivery, Work Breakdown Structure, under Grant R-263000598112 and Grant R-398000068112. Subject Editor X. Zhang.

H. Wang, Z. Xiang, and C. Lee are with the Department of Electrical and Computer Engineering, National University of Singapore, Singapore 117576 (e-mail: elelc@nus.edu.sg).

C.-F. Hu and W. Fang are with the Institute of NanoEngineering and MicroSystems, Department of Power Mechanical Engineering, National Tsing Hua University, Hsinchu 30013, Taiwan.

G. Pastorin is with the Department of Pharmacy, National University of Singapore, Singapore 117543.

Color versions of one or more of the figures in this paper are available online at http://ieeexplore.ieee.org.

Digital Object Identifier 10.1109/JMEMS.2014.2339212

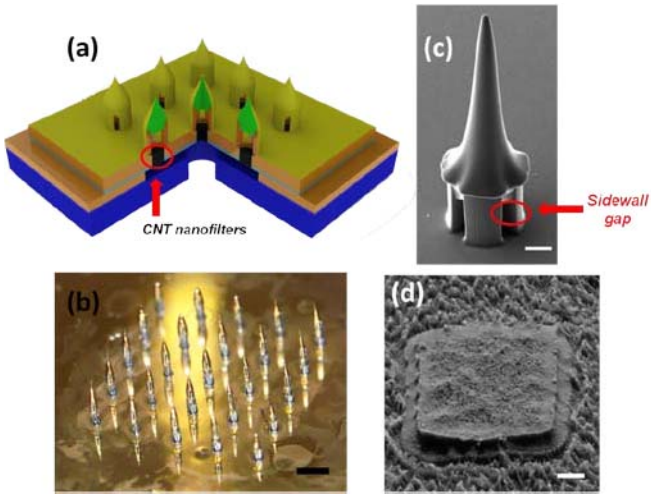

Fig. 1. 3D schematic drawing of the microneedle device integrated with CNT nanofilters; (b) Optical image of the microneedle array with gold surface electrode, scale bar is 1000 μm; (c) SEM image of single SU-8 microneedle with four-beam sidewalls and a sharp tip, scale bar is 80 μm; (d) SEM picture of a CNT bundle embedded inside the microneedle, scale bar is 10 μm.

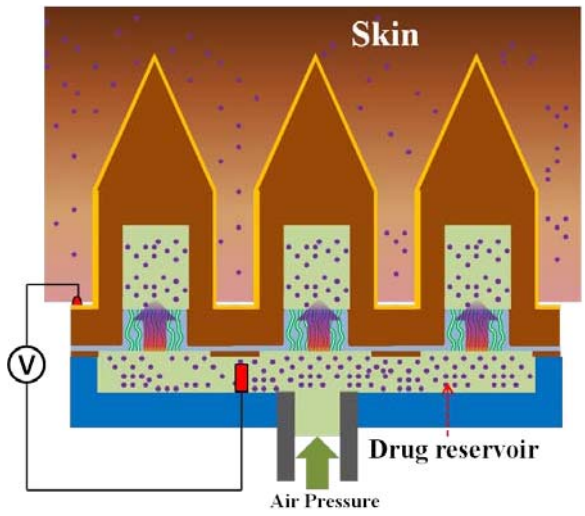

Fig. 2. Working principle of the microneedle array integrated with CNT nanofilters for transdermal drug delivery.

membrane layer and form a solution chamber. PDMS layers (the blue part in Fig. 1(a)) are bonded to the SU-8 chamber layer for tube connection in the test. Solution could be loaded in the chamber under the CNT bundles, pass through the CNT bundles and finally through the SU-8 microneedles into the tissue.

The optical image of the microneedle array with the gold surface electrode is shown in Fig. 1(b). For applying the electric field across the CNT nanofilters in the test, one electrode will be bonded onto the surface electrode and another electrode will be inserted into the PDMS chamber as shown in Fig. 2. When the solution is loaded in the drug reservoir and flow through the CNT nanofilters, two electrodes would be connected by the solution and an electric field is generated across the CNT nanofilters.

II. Device Fabrication and Characterization

A. Fabrication Process

Fig. 3 illustrates the fabrication process. The process began with thermal oxidation of single crystal silicon substrate to form a etch stop oxide layer. After the CVD of polycrystalline silicon as a sacrificial layer, a 5 nm thickness of Fe film, which acted as the catalyst film for the selective growth of CNTs, was patterned onto the silicon substrate (Fig. 3(a)). As illustrated in Fig. 3(b), the vertical aligned CNT bundles of 50 μm in height were grown via pyrolysis of acetylene at 800 °C with an Ar/NH3 flow for 15 min. As illustrated in Fig. 3(c), the CVD parylene-C was employed to fill into vertically aligned CNTs and then to reinforce the inter-tube binding at room temperature. Thus, the top side of CNTs was covered with parylene-C, and the discrete CNTs were bound together by parylene-C as show in Fig. 4(a). This step was the most critical process for forming the mechanical supporting layer for CNT bundles. The thickness of the flexible parylene-C layer was determined by the CVD process. To achieve reliable mechanical strength for the following process, a 10 μm thick parylene layer was deployed. The parylene layer was peeled off together with CNT bundles from the substrate. As shown in Fig. 3(d), the parylene film was attached onto a thin glass slide. Then a layer of 50 μm SU-8 was deposited onto the parylene layer. The thickness of this SU-8 layer was the same as the height of CNT bundles. Due to the transparency of the glass slide and parylene layer, the SU-8 layer was exposed from the back side of the glass slide. The catalyst layer under the CNT bundles could act as mask in this lithography step. The SU-8 above the CNT bundles would not be exposed. After development of SU-8, the parylene top of CNT bundles would not be covered by SU-8 as shown in Fig. 3(e) and Fig. 4(b). Such a SU-8 layer deposited above the parylene layer could act as hard mask for plasma etching. The sealed parylene top of CNT bundles could be etched by oxygen plasma as shown in Fig. 3(f) and Fig. 4(c). Then release the parylene layer together with the SU-8 cover layer from the glass slide and bonded onto an unexposed SU-8 layer deposited on another thin glass slide as shown in Fig. 3(g). In this process, a layer of SU-8 was spin coated and pre-baked on a thin glass slide first. After cooling, attach the released parylene layer onto the SU8 layer then re-bake the SU-8 layer to make it molten. After cooling, a good bonding was formed between the parylene layer and the SU-8 layer. Expose the sample from the backside of the glass slide to form a drug reservoir under the parylene layer as shown in Fig. 3(h). The size of the drug reservoir should be slightly larger than the dimension of the CNT bundle array. Etch off the catalyst layer at the backside of CNT bundles by oxygen plasma and bond it with a thin PDMS layer as shown in Fig. 3(i). For the bonding between PDMS and SU-8, the PDMS layer should be treated with nitrogen plasma then be attached onto the SU-8 layer and baked at 120 °C for 30 minutes. Then a 30 μm thick SU-8 membrane was patterned on the front layer of sample as shown in Fig. 3(j) to reinforce the structure. On this membrane layer, holes aligned with the CNT bundle array were patterned. As shown in Fig. 3(k), array of SU-8

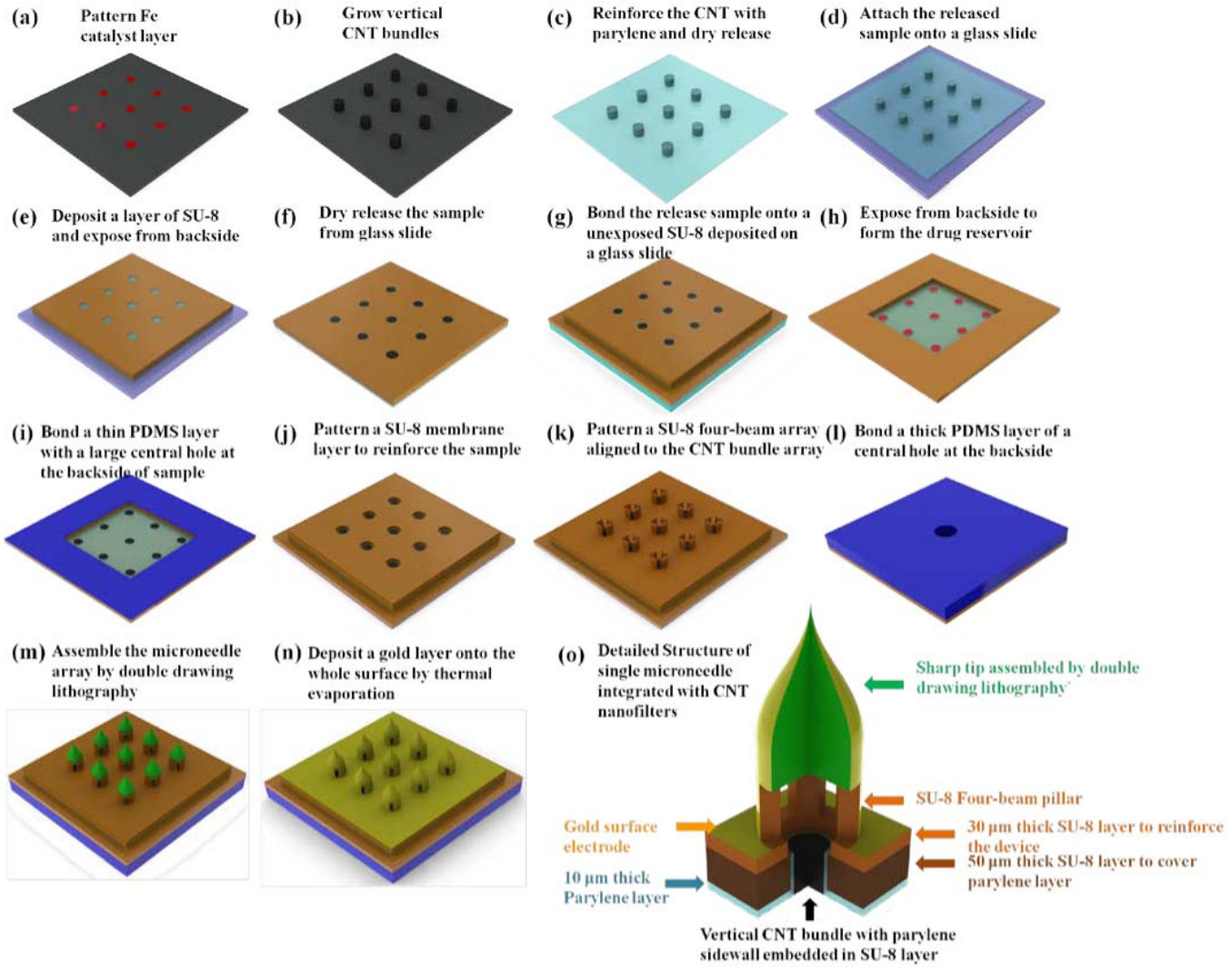

Fig. 3. Fabrication process for microneedle array integrated with CNT nanofilters: (a) Pattern Fe catalyst layer; (b) Grow vertical CNT bundles; (c) Reinforce the CNT with parylene and dry release; (d) Attach the released sample onto a glass slide; (e) Deposit a layer of SU-8 and expose from backside; (f) Dry release the sample from glass slide; (g) Bond the release sample onto an unexposed SU-8 deposited on a glass slide; (h) Expose from backside to form the drug reservoir; (i) Bond a thin PDMS layer with a large central hole at the backside of the sample; (j) Pattern a SU-8 membrane layer to reinforce the sample; (k) Pattern a SU-8 four-beam array aligned to the CNT bundle array; (l) Bond a thick PDMS layer with a central hole at the backside; (m) Assemble the microneedle array by double drawing lithography; (n)deposit a gold layer onto the whole surface by thermal evaporation; (o) Detailed structure of single microneedle integrated with CNT nanofilters.

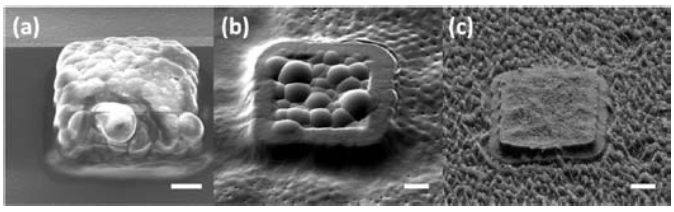

Fig. 4. (a) CNT bundle coated with parylene, the scale bar is 10 μm; (b) CNT bundle with parylene top embedded in SU-8 layer, the scale bar is 10 μm; (c) CNT bundle embedded in SU-8 layer after oxygen plasma etching, the scale bar is 10 μm.

four-beam sidewalls array was further aligned and patterned above the membrane layer. As shown in Fig. 3(i), a thick PDMS layer with a center hole was bonded at the backside. This PDMS layer was used for tubing purpose. The center hole was for the insertion of the tube. Then SU-8 sharp tips were assembled onto the four-beam sidewalls array by double drawing lithography as shown in Fig. 3(m). Finally, a gold surface electrode was deposited onto the whole surface by evaporation as shown in Fig. 3(n). The detailed structure of a single microneedle integrated with a CNT nanofilter is shown in Fig. 3(o).

B. Characterization of CNT Nanofilters

In the fabrication process, the both ends of CNT bundle need to be opened by oxygen plasma. Initially the bottom end of CNT bundle is sealed by Fe catalyst layer. Fig 5(a) shows the exposed CNTs at the bottom side after oxygen plasma treatment. Due to the property of parylene deposited by CVD, there is no parylene at the central bottom area of the CNT bundles. Fig 5(b) shows the detailed image of the exposed CNTs at the bottom end of a CNT bundle after oxygen plasma etching. There is no parylene between the CNTs.

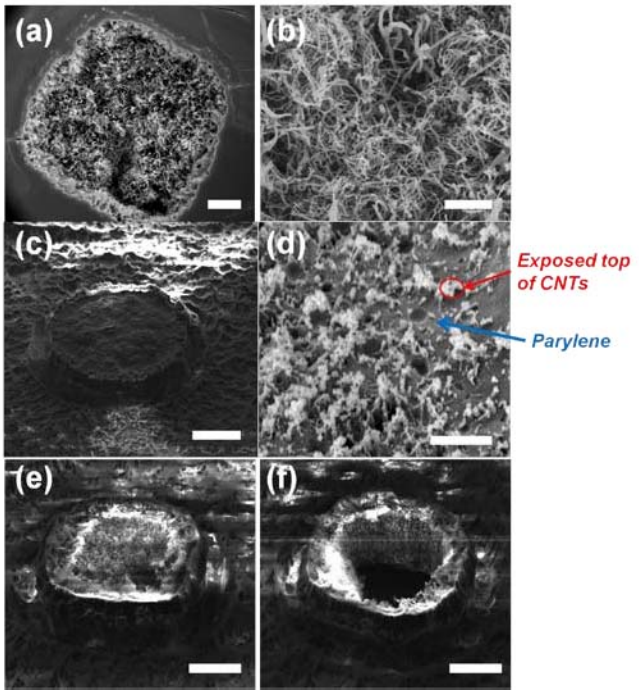

Fig. 5. (a) Backside of the CNT bundle. The catalyst layer is etched by oxygen plasma. The scale bar is 10 μm. (b) The detailed image of the backside exposed CNTs. The scale bar is 2 μm. (c) Top of the CNT bundle with proper etching dose. The scale bar is 20 μm. (d) The detailed image of the top exposed CNT. The scale bar is 2 μm. (e) Top of the CNT bundle with over etching dose. The scale bar is 20 μm. (f) After applying a air pressure, the CNT bundle within the parylene sidewall is blown away. The scale bar is 20 μm.

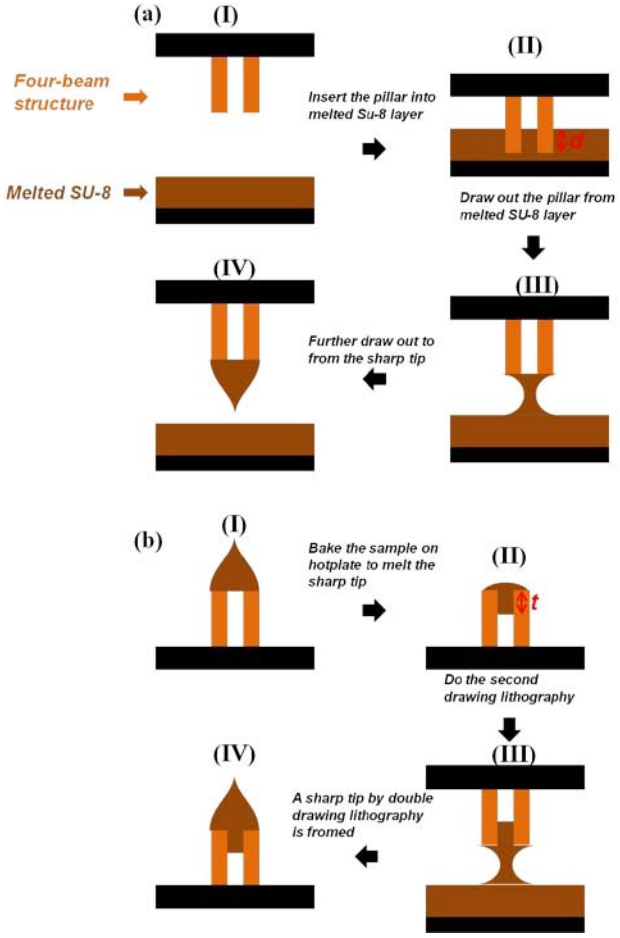

Fig. 6. (a) Process for single step drawing lithography; (b) Process for double drawing lithography, where the step I refers to the final step in the first drawing lithography, i.e., step IV in (a).

In the process of etching the top parylene layer, the proper dose of oxygen plasma is critical to make the CNTs exposed. Fig 5(c) shows the top of CNT bundle with the proper dose of oxygen plasma. Fig 5(d) shows the detailed image of the exposed CNTs. In the images, tops of individual CNTs could be seen embedded within the parylene reinforcement. No cracks between CNT and parylene were observed. The SU-8 layer around the CNT bundle was very rough after the oxygen plasma etching. Fig 5(e) shows the CNT bundles with the over dose oxygen plasma treatment. The CNTs were fully exposed and the parylene between CNTs are totally etched off. The connection between CNT bundles and parylene sidewalls became very weak. By applying a air pressure from the backside, the whole CNT bundle would be blown away as shown in Fig 5(f). To ensure the CNT bundles are etched with the proper dose of oxygen plasma, the whole etching process was divided into several cycles. The samples were checked by SEM after every cycle until only the tops of CNTs were exposed as shown in Fig 5(d).

C. Double Drawing Lithography to Assemble Microneedles Upon CNT Nanofilters

In our previous work [47], we used one time stepwise controlled drawing lithography technology for the maltose sharp tips integration. The maltose sharp tips were assembled onto hollow SU-8 tubes. We tried using the same drawing lithography process to assemble SU-8 sharp tips.

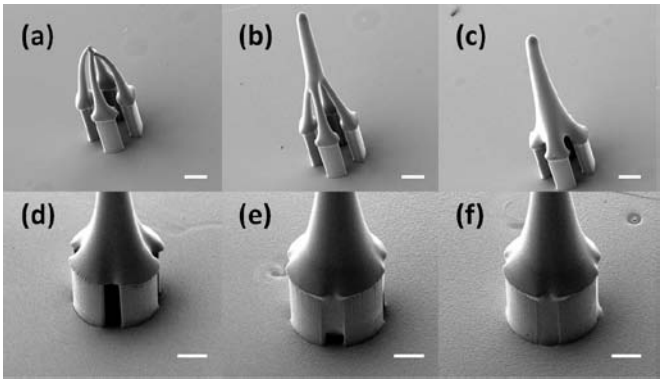

Fig. 7. (a)-(c) Results of single drawing lithography of 50 μm, 100 μm and 170 μm insertion depth; (d)-(f) Results of double drawing lithography of 10s, 30s and 60s baking time.

The process for drawing lithography is shown in Fig 6(a). A pre-baked SU-8 layer was prepared on Si substrate. Then mount the sample above the SU-8 layer and bake the SU-8 layer to make it molten as shown in step (I). Then insert the pillar into the molten SU-8 layer to a depth d as shown in step (II). Draw out the pillar from the molten SU-8 layer. Some Su-8 will attach onto the top of pillar and a Su-8 bridge

will be formed between the molten SU-8 layer and pillar as shown in step (III). Further draw out the pillar to break the SU-8 bridge and form the sharp tip as shown in step (IV).

However, the conventional drawing process can only make a hollow tip but not a solid tip structure (Fig. 7(a)–(c)). This is due to that the frame used to conduct drawing process is a four-beam structure which is different from a microtube. We changed the insertion depth d during the drawing process from 50 μm to 170 μm. This kind of tip was fragile and could not penetrate skin in practical testing process. And no matter how deep we inserted the four-beam structure into the molten SU-8 layer, the SU-8 always only attached onto the top of pillars. To solve the problem, we developed an innovative double step drawing lithography process as shown in Fig 6(b). We conducted first time stepwise controlled drawing lithography and got hollowed tips as shown in step (I). Then the whole device was baked in an oven at 120 °C to melt the hollowed SU-8 tips as shown in step (II). Molten SU-8 flowed into the gaps between four-beam sidewalls and the tips became domes. Then a second drawing process was conducted on the top of molten SU-8 to form sharp and solid tips as shown in step (III) and step (IV). The flowing depth t of the molten SU-8 in the gaps could be controlled by changing the baking time in the reflow step. The SU-8 just molten without flowing the gaps for 10s baking time (Fig. 7(d)). The SU-8 would be reflowed into the gap and block more than half of the gap for 30s baking time (Fig. 7(e)). The gap would be totally blocked with 60s baking time (Fig. 7(f)). In our chip fabrication, we just choose 10s baking time to have the gaps not blocked.

III. Experiment Results and Discussion

A. Penetration Test

Penetration tests on mouse cadaver skin were conducted to characterize the penetration capability of the SU-8 microneedles made by double drawing lithography. 10 microneedles devices were tested and no breakage was observed during the penetration. A histology image of the skin at the site of one microneedle penetration confirms that the sharp conical tip was not broken during the insertion steps. It also shows evidence of the penetration as the similar hole shape with sharp conical tip (Fig. 8).

B. Nanoparticles Blockage Test

By having the CNT nanofilters, nano-scale substance whose dimension is larger than the inner diameter of the CNT nanotube should be blocked. However, micro-scale and nano-scale cracks may occur in the parylene reinforced CNT bundles which will cause the device failure. It is necessary to verify there is no crack in the CNT nanofilters device. Due to that the whole device is made of polymer which is not suitable for TEM imaging, we leveraged fluorescent nanobeads to confirm whether the samples were crack free or not in this study.

Texas red (Sigma Aldrich, Singapore) whose molecular weight is 606.71 and fluorescent nanobead (Sigma Aldrich, Singapore) whose dimension is 80nm were mixed and delivered into the mouse skin by the microneedle devices with and without CNT nanofilters. The fluorescent images are shown in Fig. 9. For the device without CNT nanofilters, both Texas red and fluorescent nanobeads are delivered into skin as shown in Fig. 9 (a). The color of the mixed fluorescent is violet. For the device with CNT nanofilters, the skin shows red color rather than violet as shown in Fig 9 (b), which indicates only Texas red is delivered and fluorescent nanobeads are blocked. The results confirm that the CNT nanofilters could block nanobeads and there was no nano-scale crack in the CNT nanofilters. On the other hand, it has been reported that out-of-plane microneedles are not able to be inserted entirely into the skin [6], [48], [49]. During the process of delivering drug into the skin, we found that there were micrometer scale tiny gaps between bottom edge of each microneedle and skin surface due to the skin deformation as depicted in Fig. 9 (c). The skin around the edge of microneedle sidewall is in concave shape and it leaves a tiny gap at bottom part of microneedles. To investigate efficacy of microneedles in delivering drug even with the existence of these micrometer scale gaps, hydrogel absorption experiments were conducted to quantify the delivery rate and the relation between pressure and transport rate of drugs.

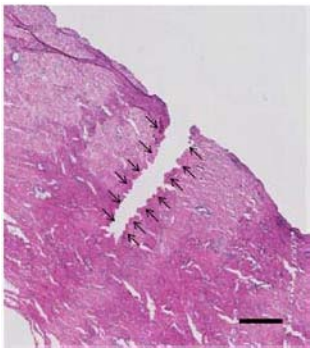

Fig. 8. Histology image of individual microneedle penetration, scale bar is 300 μm.

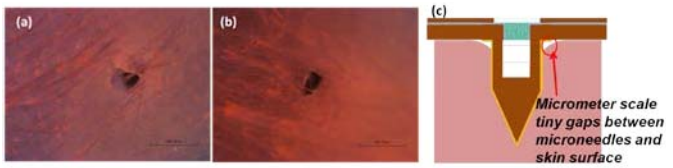

Fig. 9. Fluorescent images of mouse skin: (a) Texas red and nano-fluorescent beads are delivered with microneedle device without CNT nanofilters; (b) Texas red and nano-fluorescent beads are delivered with microneedle device with CNT nanofilters; (c) The micrometer scale gaps occur between skin and bottom edge of a microneedle due to skin deformation.

C. In Vitro Drug Delivery Test

Gelatin hydrogel was prepared by boiling 70 mL DI (Deionized) water and mixing it with 7g of gelatin powder (KnoxTM original unflavored). After cooling down, the solution was poured into a petri dish to 1cm high. Then the petri dish was put into a fridge for half an hour. The Gelatin solution became collagen slabs. The collagen slabs were cut into 6 mm×6 mm sections. A piece of fully stretched Parafilm (Parafilm M, USA) was tightly mounted on the surface of the collagen

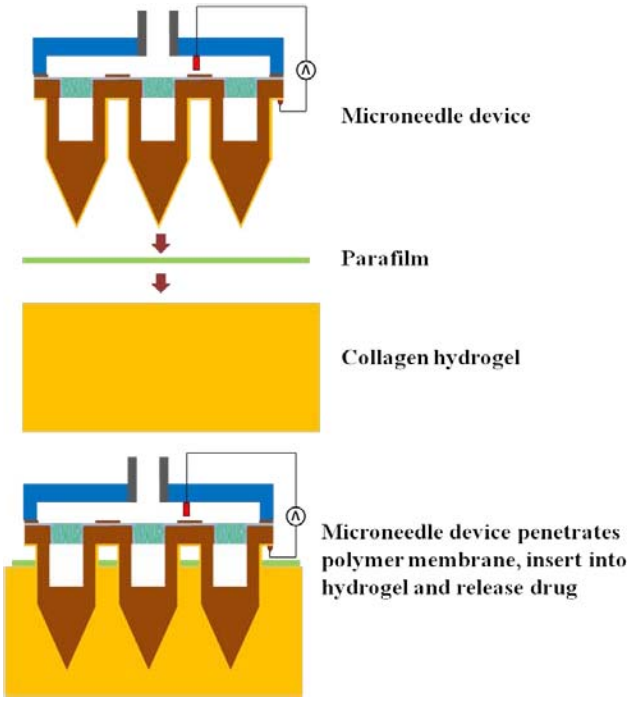

Fig. 10. Scheme describing experimental setup to test microneedle device in an in vitro hydrogel skin model. Mironeedles penetrate parafilm and collagen hydrogel to subsequently deliver drugs with controlled pressure and electric field.

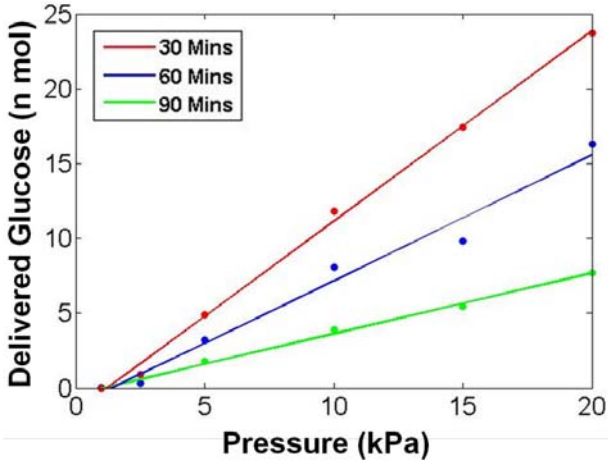

Fig. 11. Glucose delivery quantity as a function of pressure.

slabs. This parafilm was used here to block further diffusion of leaked solution into the collagen slab in the delivery process. Then the microneedles penetrated the parafilm and went into the collagen slab as shown in Fig 10. The drug could be delivered through microneedles and absorbed by the hydrogel.

In the test of glucose delivery, glucose solution was delivered into the collagen slab under different pressure and duration. Then the collagen slabs were digested in 1mg/mL collagenase (Sigma Aldrich, Singapore) at room temperature. It took around 1h for all the collagen slabs to be fully digested. The solution was collected to measure the glucose concentration with Glucose Detection kit (Abcam, Singapore). By comparing the readings from the kit with the measured concentration standard curve [52], the concentration of the glucose in hydrogel was measured. According to the glucose

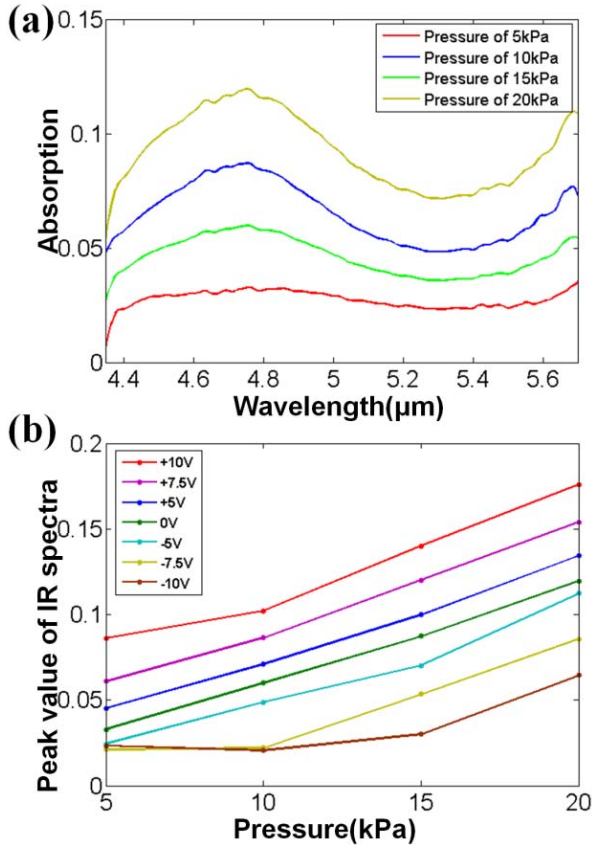

Fig. 12. Insulin delivery test result: (a) IR spectra of insulin by applying different pressure; (b) The peak value of IR spectra by applying different pressure and bias of electric field.

concentration, the absorption rate and solution delivery rate of the glucose in the hydrogel were calculated.

Fig. 11 shows that the transport rate of glucose is proportional to the given pressure and the duration of the tests. When the pressure is lower than 1 kPa, no glucose could be detected. It indicates that the CNT nanofilters could be used as a pressure valve for the delivery of glucose. The delivery rate is around 70% for all the test data. It means around 30% of the drug would leak to the surface. More importantly, after the pathways are created through the stratum corneum layer by microneedles, the drug which leaked to the skin surface eventually diffused into a deeper layer under the stratum corneum layer [50].

We conducted the same hydrogel absorption experiment for insulin. Insulin is a peptide hormone and central for regulating carbohydrate and fat metabolism in the body. Due to the poor absorption or enzymatic degradation of insulin in the gastrointestinal tract and liver, the transdermal delivery has been so far the preferred method of insulin administration. The molecular radius of insulin is 1.34nm [53] which is smaller than the inner diameter of the CNTs in the device. It could pass through the CNTs just by applying pressure. Since the insulin molecules are positively charged in the solution, the transport rate could be tuned by applying electric field.

The insulin solution of 1mg/ml concentration was preloaded in the drug reservoir. Air pressure levels in the range from 5kPa to 20kPa were applied for 30mins. The resultant solution

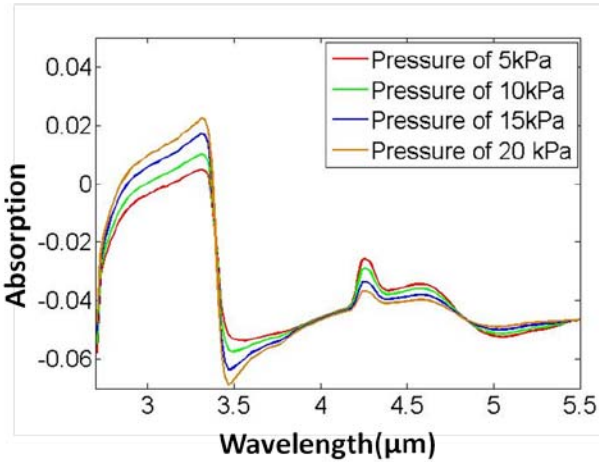

Fig. 13. IR spectra of Hemagglutinin by applying different pressure.

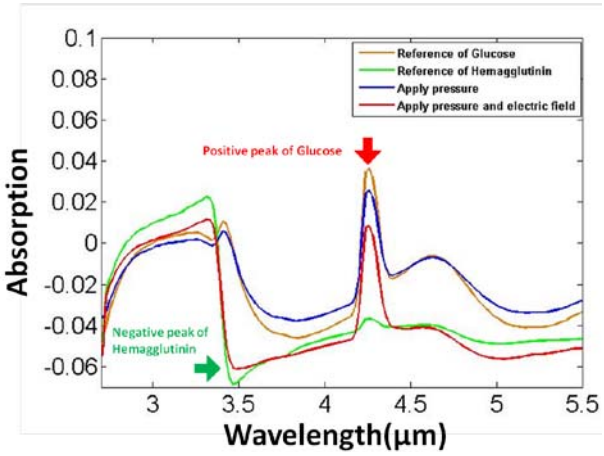

Fig. 14. IR spectra of mixture solution of difference conditions.

samples were analyzed by FTIR as shown in Fig 12(a). The peak value indicates the concentration of insulin in the sampled solutions. From the test results, the concentration of insulin is proportional to the pressure level which means the transport rate of insulin through CNTs is linear to the pressure level.

Then the test was repeated by applying bias ranges from -10V to $+10$V and air pressure ranges from 5kPa to 20kPa. The peak value of IR spectra at 4.7 μm wavelength was recorded in Fig 12(b). The positive bias could facilitate the transport of insulin and negative bias could decrease the transport rate. For the line of -7.5V and -10V, when the pressure was lower than 10kPa, the IR spectra at 4.7 μm wavelength was lower than the noise level thus no insulin was detected. This result indicates that the CNT nanofilters could be used as both pressure valve and electric switch for the delivery of insulin. And a sufficient reverse bias could balance the air pressure, realizing a zero delivery of insulin.

Hemagglutinin is a type of antibody that agglutinates red blood cells. It is a cylindrical molecule whose longitudinal dimension and diameter are is 13.5 and 6.5nm, respectively [51]. Because the length of the molecule, 13.5nm, is larger than the inner diameter of the CNT nanotubes, 10nm, the Hemagglutinin cannot pass through the CNT just by applying pressure.

According to our previous study [46], Hemagglutinin can pass through the CNTs when both electric field and pressure are applied together. This is because the cylindrical molecule can be aligned by the DEP force.

In the test, we applied 5V bias for 1 hour. The pressure changes from 5kPa to 20kPa. The sample solution was analyzed with FTIR. The IR spectra were shown in Fig. 13. Due to that we used a water based solution as background for FTIR analysis, some negative peaks occurred in the spectra meaning the absorption was lower than water at that wavelength. The peak value was not in proportion to the pressure which indicates that the transport rate of large molecules is not proportional to the pressure. No heamagglutinin was detected when no electric field was applied. Therefore, the CNT nanofilters could act as a electric switch for the delivery of heamagglutinin.

The transport conditions of glucose and Hemagglutinin through CNT nanofilters are different. So if glucose and Hemagglutinin are mixed together, a selective transport could be realized by controlling the pressure and electric field applied. Then we mixed the glucose and Hemagglutinin together and conducted the test again. In one test, only 20kPa pressure was applied. In another test 5V bias and 20kPa pressure were applied. The durations of both tests were one hour. The IR spectra were shown in Fig. 14. The green line is the reference of Hemagglutinin and the brown line is the reference of glucose. For Hemagglutinin, there is a negative peak at 3.5 μm. For glucose, there is a positive peak at 4.3 μm. When only pressure was applied, only glucose was detected. The blue line shows the similar curve as the brown line without the negative peak at 3.5 μm. When both pressure and electric field were applied, both Hemagglutinin and glucose could be detected. The red line indicates both the negative peak at 3.5 μm. and positive peak at 4.3 μm. This result confirms that by controlling the conditions, Hemagglutinin could be selectively delivered while glucose could always be delivered.

IV. Conclusion

A microneedle array integrated with CNT nanofilters for realization of controlled and selective drug delivery has been reported. The SU-8 tips made by the double drawing lithography process are sharp and stiff enough to penetrate skin. Nanobeads of 80 nm diameter were blocked in the test. It indicates there were no nano-scale cracks in the device and the CNT nanofilters could block all substance larger than its inner diameter. The device could be used for controlled selective transdermal drug delivery. The transport rate of glucose and insulin of low molecular weight is proportional to the pressure given. But the transport rate of Hemagglutinin, i.e., a large molecule, is not in proportion to the pressure. The transport rate of charged molecule such as insulin could be tuned by an electric field. For the molecule which could be aligned by DEP force to pass through the CNT inner channel, CNT nanofilters could be used as an electrical switch. When the molecule is much smaller than the inner diameter of the CNTs, CNT

nanofilters could be used as a pressure valve. The function of drug administration could be implemented by having the CNT nanofilters in microneedle array. It could expand the application of microneedles for a long term automatically disease monitoring and drug delivery system.

REFERENCES

[1] M. R. Prausnitz, "Microneedles for transdermal drug delivery," *Adv. Drug Del. Rev.*, vol. 56, no. 5, pp. 581–587, 2004.

[2] N. Wilke, A. Mulcahy, S.-R. Ye, and A. Morrissey, "Process optimization and characterization of silicon microneedles fabricated by wet etch technology," *Microelectron. J.*, vol. 36, no. 7, pp. 650–656, 2005.

[3] H. S. Gill, D. D. Denson, B. A. Burris, and M. R. Prausnitz, "Effect of microneedle design on pain in human volunteers," *Clin. J. Pain*, vol. 24, no. 7, pp. 585–594, 2008.

[4] J. A. Matriano *et al.*, "Macroflux microprojection array patch technology: A new and efficient approach for intracutaneous immunization," *Pharmaceutical Res.*, vol. 19, no. 1, pp. 63–70, 2002.

[5] T. Omatsu *et al.*, "Metal microneedle fabrication using twisted light with spin," *Opt. Exp.*, vol. 18, no. 17, pp. 17967–17973, 2010.

[6] I. Mansoor, Y. Liu, U. O. Häfeli, and B. Stoeber, "Arrays of hollow out-of-plane microneedles made by metal electrodeposition onto solvent cast conductive polymer structures," *J. Micromech. Microeng.*, vol. 23, no. 8, p. 085011, 2013.

[7] M. Yang and J. D. Zahn, "Microneedle insertion force reduction using vibratory actuation," *Biomed. Microdevices*, vol. 6, no. 3, pp. 177–182, 2004.

[8] C. Y. Jin, M. H. Han, S. S. Lee, and Y. H. Choi, "Mass producible and biocompatible microneedle patch and functional verification of its usefulness for transdermal drug delivery," *Biomed. Microdevices*, vol. 11, no. 6, pp. 1195–1203, 2009.

[9] K. A. Moga *et al.*, "Rapidly–dissolvable microneedle patches via a highly scalable and reproducible soft lithography approach," *Adv. Mater.*, vol. 25, no. 36, pp. 5060–5066, 2013.

[10] P. C. Wang, S. J. Paik, S. D. Chen, S. Rajaraman, S. H. Kim, and M. G. Allen, "Fabrication and characterization of polymer hollow microneedle array using UV lithography into micromolds," *J. Microelectromech. Syst.*, vol. 22, no. 5, pp. 1041–1053, Oct. 2013.

[11] R. Wang, W. Zhao, W. Wang, and Z. Li, "Fabrication and properties of 3D flexible parylene-based microelectrode array with silicon tips," in *Proc. IEEE 24th Int. Conf. Micro Electro Mech. Syst. (MEMS)*, Cancun, Mexico, Jan. 2011, pp. 253–256.

[12] R. Wang, X. Huang, G. Liu, W. Wang, F. Dong, and Z. Li, "Fabrication and characterization of a parylene-based three-dimensional microelectrode array for use in retinal prosthesis," *J. Microelectromech. Syst.*, vol. 19, no. 2, pp. 367–374, 2010.

[13] H. Yu, N. Zheng, W. Wang, S. Wang, X. Zheng, and Z. Li, "Electroplated nickel multielectrode microprobes with flexible parylene cable for neural recording and stimulation," *J. Microelectromech. Syst.*, vol. 22, no. 5, pp. 1199–1206, 2013.

[14] R. Wang, W. Zhao, W. Wang, and Z. Li, "A flexible microneedle electrode array with solid silicon needles," *J. Microelectromech. Syst.*, vol. 21, no. 5, pp. 1084–1089, 2012.

[15] C.-J. Ke *et al.*, "Multidrug release based on microneedle arrays filled with pH-responsive PLGA hollow microspheres," *Biomaterials*, vol. 33, no. 20, pp. 5156–5165, 2012.

[16] H. Huang and C. Fu, "Different fabrication methods of out-of-plane polymer hollow needle arrays and their variations," *J. Micromech. Microeng.*, vol. 17, no. 2, pp. 393–402, 2007.

[17] Y. Choi, M. A. McClain, M. C. LaPlaca, A. B. Frazier, and M. G. Allen, "Three dimensional MEMS microfluidic perfusion system for thick brain slice cultures," *Biomed. Microdevices*, vol. 9, no. 1, pp. 7–13, 2007.

[18] S. P. Davis, W. Martanto, M. G. Allen, and M. R. Prausnitz, "Hollow metal microneedles for insulin delivery to diabetic rats," *IEEE Trans. Biomed. Eng.*, vol. 52, no. 5, pp. 909–915, May 2005.

[19] P.-C. Wang, B. A. Wester, S. Rajaraman, S.-J. Paik, S.-H. Kim, and M. G. Allen, "Hollow polymer microneedle array fabricated by photolithography process combined with micromolding technique," in *Proc. 31st Annu. Int. Conf. IEEE Eng. Med. Biol. Soc.*, Minneapolis, MN, USA, Sep. 2009, pp. 7026–7029.

[20] S. Rajaraman *et al.*, "Three-dimensional metal transfer micromolded microelectrode arrays (MEAS) for in-vitro brain slice recordings," in *Proc. TRANSDUCERS*, Lyon, France, 2007, pp. 1251–1254.

[21] S. Rajaraman, J. A. Bragg, J. D. Ross, and M. G. Allen, "Micromachined three-dimensional electrode arrays for transcutaneous nerve tracking," *J. Micromech. Microeng.*, vol. 21, no. 8, p. 085014, 2011.

[22] K. Lee and H. Jung, "Drawing lithography for microneedles: A review of fundamentals and biomedical applications," *Biomaterials*, vol. 33, no. 30, pp. 7309–7326, 2012.

[23] K. Lee, J. D. Kim, C. Y. Lee, S. Her, and H. Jung, "A high-capacity, hybrid electro-microneedle for *in-situ* cutaneous gene transfer," *Biomaterials*, vol. 32, no. 30, pp. 7705–7710, 2011.

[24] K. Lee, C. Y. Lee, and H. Jung, "Dissolving microneedles for transdermal drug administration prepared by stepwise controlled drawing of maltose," *Biomaterials*, vol. 32, no. 11, pp. 3134–3140, 2011.

[25] M. Majumder, N. Chopra, and B. J. Hinds, "Mass transport through carbon nanotube membranes in three different regimes: Ionic diffusion and gas and liquid flow," *ACS Nano*, vol. 5, no. 5, pp. 3867–3877, 2011.

[26] P. Krishnakumar *et al.*, "Mass transport through vertically aligned large diameter MWCNTs embedded in parylene," *Nanotechnology*, vol. 23, no. 45, p. 455101, 2012.

[27] Z. W. Ulissi, S. Shimizu, C. Y. Lee, and M. S. Strano, "Carbon nanotubes as molecular conduits: Advances and challenges for transport through isolated sub-2 nm pores," *J. Phys. Chem. Lett.*, vol. 2, no. 22, pp. 2892–2896, 2011.

[28] W. Reisner, J. N. Pedersen, and R. H. Austin, "DNA confinement in nanochannels: Physics and biological applications," *Rep. Progr. Phys.*, vol. 75, no. 10, p. 106601, 2012.

[29] D. Cai *et al.*, "A molecular-imprint nanosensor for ultrasensitive detection of proteins," *Nature Nanotechnol.*, vol. 5, pp. 597–601, Jun. 2010.

[30] A. Noy, H. Park, F. Fornasiero, J. Holt, C. Grigoropoulos, and O. Bakajin, "Nanofluidics in carbon nanotubes," *Nanotoday*, vol. 2, no. 6, pp. 22–29, 2007.

[31] C. Y. Lee, W. Choi, J.-H. Han, and M. S. Strano, "Coherence resonance in a single-walled carbon nanotube ion channel," *Science*, vol. 329, no. 5997, pp. 1320–1324, 2010.

[32] Q. Zhou and L. Lin, "Enhancing mass transport for synthesizing single-walled carbon nanotubes via micro chemical vapor deposition," *J. Microelectromech. Syst.*, vol. 20, no. 1, pp. 9–11, 2011.

[33] H. Liu *et al.*, "Translocation of single-stranded DNA through single-walled carbon nanotubes," *Science*, vol. 327, no. 5961, pp. 64–67, 2010.

[34] M. Sun and Y. Gao, "Electrically driven gallium movement in carbon nanotubes," *Nanotechnology*, vol. 23, no. 6, p. 065704, 2012.

[35] J. Zhao, J. Q. Huang, F. Wei, and J. Zhu, "Mass transportation mechanism in electric-biased carbon nanotubes," *Nano Lett.*, vol. 10, no. 11, pp. 4309–4315, 2010.

[36] J. He, H. Liu, P. Pang, D. Cao, and S. Lindsay, "Translocation events in a single-walled carbon nanotube," *J. Phys., Condens. Matter*, vol. 22, no. 45, p. 454112, 2010.

[37] P. Pang, J. He, J. Park, P. Krstić, and S. Lindsay, "Origin of giant ionic currents in carbon nanotube channels," *ACS Nano*, vol. 5, no. 9, pp. 7277–7283, 2011.

[38] X. Qin, Q. Yuan, Y. Zhao, S. Xie, and Z. Liu, "Measurement of the rate of water translocation through carbon nanotubes," *Nano Lett.*, vol. 11, no. 5, pp. 2173–2177, 2011.

[39] J. K. Holt, "Carbon nanotubes and nanofluidic transport," *Adv. Mater.*, vol. 21, no. 35, pp. 3542–3550, 2009.

[40] D. Mattia and Y. Gogotsi, "Review: Static and dynamic behavior of liquids inside carbon nanotubes," *Microfluidics Nanofluidics*, vol. 5, no. 3, pp. 289–305, 2008.

[41] M. Whitby, L. Cagnon, M. Thanou, and N. Quirke, "Enhanced fluid flow through nanoscale carbon pipes," *Nano Lett.*, vol. 8, no. 9, pp. 2632–2637, 2008.

[42] C. Shearer *et al.*, "Water transport through nanoporous materials: Porous silicon and single walled carbon nanotubes," in *Proc. Int. Conf. Nanosci. Nanotechnol.*, Feb. 2010, pp. 196–199.

[43] H. Verweij, M. C. Schillo, and J. Li, "Fast mass transport through carbon nanotube membranes," *Small*, vol. 3, no. 12, pp. 1996–2004, 2007.

[44] L. Zhang *et al.*, "Gas transport in vertically-aligned carbon nanotube/parylene composite membranes," *Carbon*, vol. 66, pp. 11–17, Jan. 2013.

[45] X. Sun, X. Su, J. Wu, and B. J. Hinds, "Electrophoretic transport of biomolecules through carbon nanotube membranes," *Langmuir*, vol. 27, no. 6, pp. 3150–3156, 2011.

[46] H. Wang *et al.*, "Development of stretchable membrane based nanofilters using patterned arrays of vertically grown carbon nanotubes," *Nanoscale*, vol. 5, no. 18, pp. 8488–8493, 2013.

[47] Z. Xiang, H. Wang, A. Pant, G. Pastorin, and C. Lee, "Development of vertical SU-8 microtubes integrated with dissolvable tips for transdermal drug delivery," *Biomicrofluidics*, vol. 7, no. 2, p. 026502, 2013.
[48] N. Roxhed, T. C. Gasser, P. Griss, G. A. Holzapfel, and G. Stemme, "Penetration-enhanced ultrasharp microneedles and prediction on skin interaction for efficient transdermal drug delivery," *J. Microelectromech. Syst.*, vol. 16, no. 6, pp. 1429–1440, 2007.
[49] D. V. McAllister *et al.*, "Microfabricated needles for transdermal delivery of macromolecules and nanoparticles: Fabrication methods and transport studies," *Proc. Nat. Acad. Sci. United States Amer.*, vol. 100, no. 24, pp. 13755–13760, 2007.
[50] N. Wilke, A. Mulcahy, S. R. Ye, and A. Morrissey, "Process optimization and characterization of silicon microneedles fabricated by wet etch technology," *Microelectron. J.*, vol. 36, no. 7, pp. 650–656, 2005.
[51] C. Böttcher, K. Ludwig, A. Herrmann, M. V. Heel, and H. Stark, "Structure of influenza haemagglutinin at neutral and at fusogenic pH by electron cryo-microscopy," *FEBS Lett.*, vol. 463, no. 3, pp. 255–259, 1999.
[52] *Glucose Detection Kit Data Sheet*. [Online]. Available: http://www.abcam.com/glucose-detection-kit-ab102517.html
[53] P. R. Shorten, C. D. McMahon, and T. K. Soboleva, "Insulin transport within skeletal muscle transverse tubule networks," *Biophys. J.*, vol. 93, no. 9, pp. 3001–3007, 2007.

Hao Wang received the B.Eng. degree from the School of Optoelectronic Information, University of Electronic Science and Technology of China, Chengdu, China, in 2010. He is currently a Research Engineer of Electrical Communication Engineering with the National University of Singapore, Singapore, where he is currently pursuing the M.Eng. degree with the Department of Electrical Communication Engineering. His research interests are focused on nanoneedle devices for transdermal drug delivery.

Zhuolin Xiang received the B.Eng. degree from the Department of Information and Electronics, Beijing Institute of Technology, Beijing, China, in 2011. He is currently pursuing the Ph.D. degree in electrical and computer engineering with the National University of Singapore, Singapore. His research interests focus mainly on bioMEMs devices for drug delivery and neural interfacing.

Chih-Fan Hu was born in Taipei, Taiwan, in 1982. He received the Ph.D. degree from the National Tsing Hua University, Hsinchu, Taiwan, in 2013.

He is currently a Research and Development Engineer with the United Microelectronics Corporation, Hsinchu. His research interests include MEMS pressure sensors, flexible sensors, and CNTs-based sensors.

Giorgia Pastorin received the Ph.D. degree in medicinal chemistry in Italy in 2004, and then specialized in drug delivery through the use of functionalized nanomaterials for several biomedical applications. She is currently an Associate Professor with the Department of Pharmacy, National University of Singapore, Singapore, where she is responsible for the Bio Laboratory at NanoCore.

She has published more than 70 research papers and reviews in internationally recognized journals, including *Nature Nanotechnology*, *Proceedings of the National Academy of Sciences*, *Nano Letters*, and *Angewandte Chemie International Edition*.

Weileun Fang was born in Taipei, Taiwan. He received the Ph.D. degree from Carnegie Mellon University, Pittsburgh, PA, USA, in 1995. In 1995, he was a Post-Doctoral Researcher with the Synchrotron Radiation Research Center, Hsinchu, Taiwan. He joined the Department of Power Mechanical Engineering with the National Tsing Hua University, Hsinchu, in 1996, where he is currently a Distinguished Professor and a faculty member of the Institute of NanoEngineering and MicroSystems. In 1999, he was with Prof. Y. C. Tai at the California Institute of Technology, Pasadena, CA, USA, as a Visiting Associate. His research interests include microelectromechanical systems (MEMS) with an emphasis on micro fabrication/packaging technologies, complementary metal–oxide–semiconductor MEMS, carbon nanotubes MEMS, microoptical systems, micro sensors and actuators, and characterization of thin-film mechanical properties. He has published more than 140 Science Citation Index journal papers, about 250 international conference papers, and holds 80 patents (all in MEMS field). He is currently the Editor-in-Chief of *Journal of Micromechanics and Microengineering*, a Board Member of the IEEE TRANSACTIONS ON DEVICE AND MATERIALS RELIABILITY, and an Associate Editor of the IEEE SENSORS JOURNAL and *Sensors and Actuators A*. He served as the Chief Delegate of the Taiwan of World Micromachine Summit from 2008 to 2012, the Chair of MMS 2012, the Technical Program Committee of the IEEE Micro Electro Mechanical Systems Conference, the EPC of Transducers Conference, and the Regional Co-Chair and the TPC Chair of the IEEE Sensors Conference. He has been a member of the International Steering Committee of Transducers since 2009. He also serves as a Technical Consultant for many MEMS companies in Taiwan.

Chengkuo Lee (M'96) received the M.S. degree in materials science and engineering from National Tsing Hua University, Hsinchu, Taiwan, in 1991; the M.S. degree in industrial and system engineering from Rutgers University, New Brunswick, NJ, USA, in 1993; and the Ph.D. degree in precision engineering from the University of Tokyo, Tokyo, Japan, in 1996. He was a Foreign Researcher with the Nanometerscale Manufacturing Science Laboratory, Research Center for Advanced Science and Technology, University of Tokyo, from 1993 to 1996. He was with the Mechanical Engineering Laboratory, Advanced Industrial Science and Technology, Ministry of International Trade and Industry, Japan, as a JST Research Fellow, in 1996. He was a Senior Research Staff Member with the Microsystems Laboratory, Industrial Technology Research Institute, Hsinchu. In 1997, he joined Metrodyne Microsystem Corporation, Hsinchu, and established the Microelectromechanical Systems (MEMS) Device Division and the first micromachining fabrication for commercial purposes in Taiwan. He was the Manager of the MEMS Device Division from 1997 to 2000; an Adjunct Assistant Professor with the Department of Electro-Physics, National Chiao Tung University, Hsinchu, in 1998; and an Adjunct Assistant Professor with the Institute of Precision Engineering, National Chung Hsing University, Taichung, Taiwan, from 2001 to 2005. In 2001, he co-founded Asia Pacific Microsystems, Inc., Hsinchu, where he became the Vice President of Research and Development before becoming the Vice President of the Optical Communication Business Unit, and a Special Assistant to the Chief Executive Officer in charge of international business and technical marketing for the MEMS foundry service. He was a Senior Member of the Technical Staff with the Institute of Microelectronics, Agency for Science, Technology and Research, Singapore, from 2006 to 2009. He is currently an Associate Professor with the Department of Electrical and Computer Engineering, National University of Singapore, Singapore. He co-authored *Advanced MEMS Packaging* (McGraw-Hill, 2010), and contributed more than 220 international conference papers and extended abstracts and 150 peer-reviewed international journal articles in the fields of sensors, actuators, energy harvesting, MEMS, nanoelectromechanical systems, nanophotonics, and nanotechnology. He holds nine U.S. patents.